Bioorganic Chemistry 112 (2021) 104963

Contents lists available at ScienceDirect

Bioorganic Chemistry

journal homepage: www.elsevier.com/locate/bioorg

Discovery of pseudolaric acid A as a new Hsp90 inhibitor uncovers its potential anticancer mechanism

Jiangxin Liu [1], Xing-De Wu [1], Wenyan Li [1], Zaifeng Yuan [1], Kun Yang, Qin-Shi Zhao [*]

State Key Laboratory of Phytochemistry and Plant Resources in West China, Kunming Institute of Botany, Chinese Academy of Sciences, Kunming 650201, China

ARTICLE INFO

Keywords:
Pseudolaric acid A
Hsp90 inhibitor
Apoptosis
NMR
Structure-activity relationship
Photoaffinity-based probe
Protein-ligand interaction

ABSTRACT

Pseudolaric acid A (PAA), one of the main bioactive ingredients in traditional medicine *Pseudolarix cortex*, exhibits remarkable anticancer activities. Yet its mechanism of action and molecular target have not been investigated and remain unclear. In this work, mechanistic study showed that PAA induced cell cycle arrest at G2/M phase and promoted cell death through caspase-8/caspase-3 pathway, demonstrating potent antiproliferation and anticancer activities. PAA was discovered to be a new Hsp90 inhibitor and multiple biophysical experiments confirmed that PAA directly bind to Hsp90. Active PAA-probe was designed, synthesized and biological evaluated. It was subsequently employed to verify the cellular interaction with Hsp90 in HeLa cells through photoaffinity labeling approach. Furthermore, NMR experiments showed that *N*-terminal domain of Hsp90 and essential groups in PAA are important for the protein-inhibitor recognition. Structure-activity relationship studies revealed the correlation between its Hsp90 inhibitory activity with anticancer activity. This work proposed a potential mechanism involved with the anticancer activity of PAA and will improve the appreciation of PAA as a potential cancer therapy candidate.

1. Introduction

Natural products, exhibiting rich structural diversity, complexity and high degree of stereochemistry, have been the rich and invaluable compound sources for drug discovery. Particularly, they are major sources of innovative anticancer and antimicrobial therapeutic agents [1]. Molecular target identification and mechanisms of action are the key steps for the natural product-based drug discovery and determination of potential efficacy [2,3]. During recent decades, the molecular targets of several natural compounds have been successfully identified, such as celastrol [4], artemisinin [5], and bile acid [6]. Photoaffinity labeling (PAL), using a chemical probe to covalently bind to its target, is a powerful technique to identify unknown targets of small molecules, study protein-ligand interactions, and probe the location of binding sites in drug discovery [7,8]. The general design strategy of photoaffinity probe involves the incorporation of three important functionalities, including compound of interest, photoreactive moiety and/or affinity tag [9]. Structure-activity relationship (SAR) analysis is often required to evaluate whether the chemical probes retain the bioactivity. Click chemistry-based PAL is increasingly popular and described in many successful examples [6,10,11]. Terminal alkyne, one of the smallest and least perturbing "clickable" tag, can be ligated to an azide-functionalized moiety via copper-catalyzed azide-alkyne cycloaddition [12]. This ligation was successfully applied for the enrichment of cellular targets.

Interest in natural products from traditional medicine is increasing as the technological advances [13]. *Pseudolarix cortex*, the processed and dried root and trunk barks of *Pseudolarix amabilis* (Nelson) Rehd. (Figure S1), has been employed in clinical practice for centuries and prescribed as antifungal agent to treat fungal skin infection since the 17th century [14]. Pseudolaric acid A (PAA, Figure S1), a unique tricyclic diterpenoid, is one of the main components and major bioactive ingredient of this species [15]. Bioactivity studies demonstrate that PAA exhibits considerable cytotoxicity towards a variety of cell lines and anticancer activity, indicating the potential value as an anticancer drug lead [16,17]. Even though *Pseudolarix cortex* has long been used in traditional medicine with PAA being one of the active components, mechanism responsible for PAA exerting the biological function is not clear. Extensive studies are needed to address the following concerns: its potential anti-cancer mechanism, biological targets, and the coupling of

* Corresponding author.
E-mail address: qinshizhao@mail.kib.ac.cn (Q.-S. Zhao).
[1] These authors contributed equally.

https://doi.org/10.1016/j.bioorg.2021.104963
Received 26 March 2021; Received in revised form 27 April 2021; Accepted 1 May 2021
Available online 5 May 2021

activity with target engagement.

Heat shock protein 90 (Hsp90) is a molecular chaperon essential for the cell viability, promoting the correct folding and assembling of its client proteins [18]. Hsp90 levels and functions were elevated in tumor cells. The expression level of Hsp90 is 2- to 10- fold higher in tumor cells than that in the normal cells. Cancer cells utilized the chaperon machinery to protect the mutated oncoproteins from misfolding and degradation [19]. >300 client proteins of Hsp90 have been reported and play important roles in many oncogenic processes and hallmarks of cancer, including Akt involved in the PI3 kinase signaling and CDK-4 involved in the cell cycle regulation [20]. The Hsp90-dependent client proteins are highly involved in regulating the cell cycle, stimulating cell proliferation and inhibiting cell apoptosis [21]. In cancer cells, unrestricted proliferation and suppressed apoptosis are the two critical factors responsible for the cancer cells growing malignantly [22]. Given the essential roles of client proteins of Hsp90 in cancer cells, inhibition of Hsp90 has been an important drug discovery strategy for cancer treatment [23]. Several natural products are established to be Hsp90 inhibitors, such as antitumor antibiotics geldanamycin [24], radicicol [25] and 5-aryl-3-thiophen-2-yl-1H-pyrazoles [26]. Our group previously reported vibsanin B derivatives as Hsp90 C-terminal inhibitors [27]. An array of inhibitors targeting the *N*-terminal ATP binding pocket of Hsp90 is evaluated for anticancer activities in patients. Considering the high degree of structural plasticity of Hsp90 and signal propagation between N- and C-terminal domains which may induce an allosteric regulation of the chaperon complex [28], widespread efforts in recent years have been focused on the allosteric site drug discovery and small molecules targeting of protein-protein interaction (PPIs) [29].

In this present study, PAA induced cell cycle arrest at G2/M phase and promoted the cell apoptosis through caspase-8/caspase-3 pathway in HeLa cells. We further discovered PAA as the new Hsp90 inhibitor and biochemically validated PAA binding to *N*-terminal domain (NTD) of Hsp90. A photoactive chemical probe was employed to verify the cellular interaction with Hsp90 in HeLa cells through photoaffinity labeling approach. The anti-cancer activity of PAA is well correlated to its Hsp90 inhibitory activity through structure-activity relationship analysis.

2. Results and discussion

2.1. PAA induced cell cycle arrest at G2/M phase and apoptosis

To investigate the possible mechanism of anticancer activity of PAA, cell growth inhibition effect of PAA was studied. Cell cycle distribution and cell apoptosis analysis on HeLa cells were carried out. We treated HeLa cells with different concentrations of PAA, and measured the cell population in each phase of the cell cycle using the flow cytometry. PAA treatment caused an obvious reduction of cells in G0-G1 phase and the concomitant increase of cells in G2/M phase in the dose-dependent manner (Fig. 1A and 1C). ~93% ($p < 0.05$) of the cells are arrested in

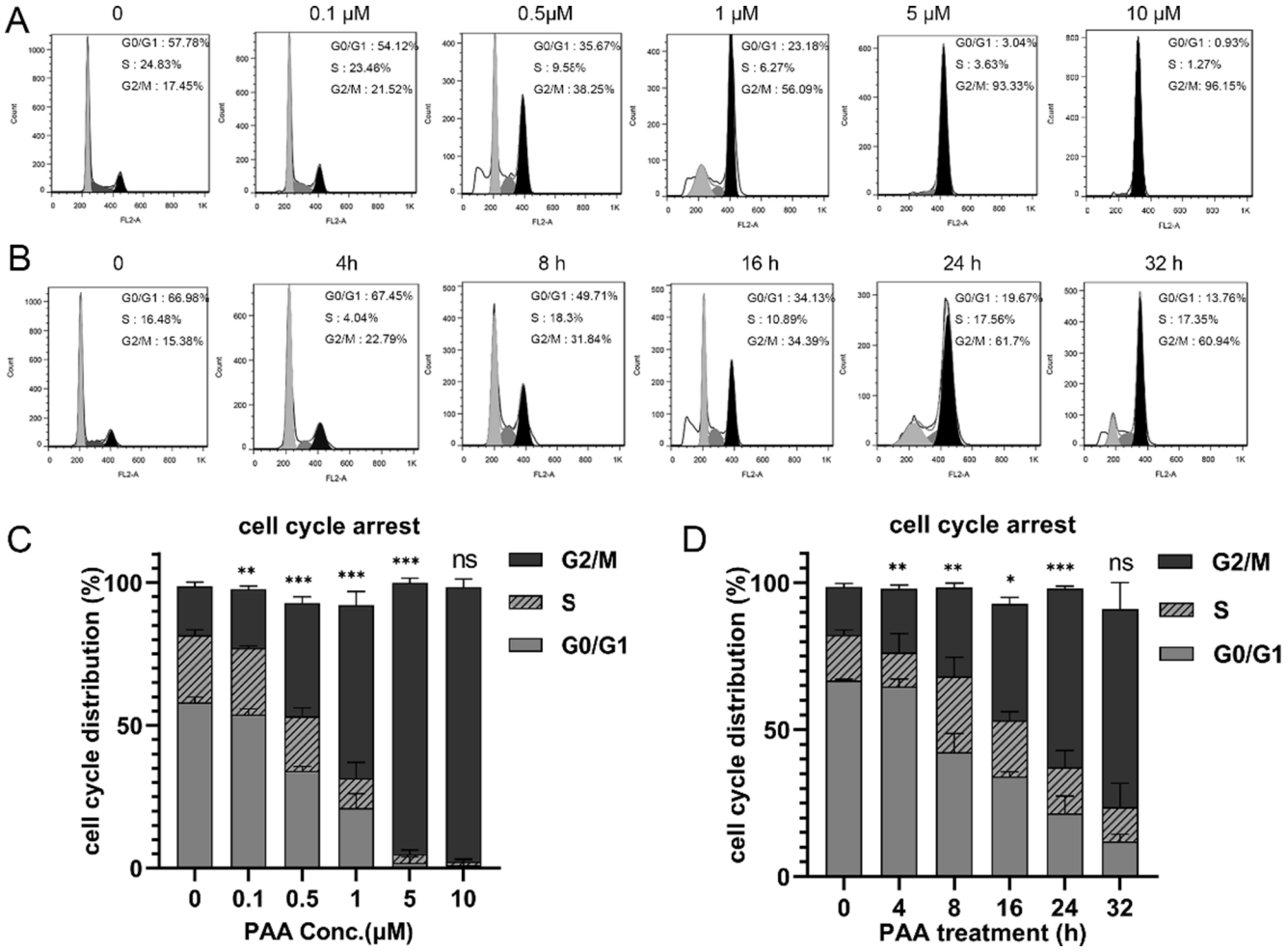

Fig. 1. PAA induced the G2/M phase arrest in HeLa cells in the concentration and time dependent manner. The cell cycles were evaluated by flow cytometric analysis. (A) HeLa cells were incubated with different concentrations of PAA for 16 h. (B) HeLa cells were treated with 0.5 μM of PAA for different time points. (C) Quantitative analysis of cell cycle distribution in each cell cycle phase at indicated concentration of PAA. (D) The quantified bar graph of cell population at indicated time points. (*$p < 0.05$; ** $p < 0.01$; *** $p < 0.001$) vs previous data point; ns, not significant; Data are the representative of three independent experiments).

the G2/M phase with 5 μM PAA. Strikingly, the percentage of cells in the G2/M phase increased in the time-dependent manner as well (Fig. 1B and 1D). These results illustrated that PAA stimulated the cell cycle arrest at G2/M phase and inhibited cell proliferation in HeLa cells.

Subsequently, we investigated whether PAA treatment promoted cell death. Annexin V binding and propidium iodide (PI) uptake followed by flow cytometry is robust assay to detect and quantify apoptotic and necrotic cells [30]. Results showed that PAA stimulated the apoptotic cell death in the dose-dependent manner (Fig. 2A and 2B). ~ 48.3% of the cells were in the apoptotic stage and 5.22% of the cells in the necrotic stage after treatment of 5 μM PAA. Percentage of cells in apoptosis were significantly higher than that of necrotic cells in each PAA concentration point. The data provided evidence to support the concept that PAA showed the anticancer activity through suppressing cell proliferation and promoting cell apoptosis.

2.2. Apoptotic mechanism studies

To gain further insight into the PAA-caused apoptosis, we assessed the expression profile of apoptotic-related marker proteins. The induction of apoptosis was accompanied by two marker events: activation/cleavage of caspase-3 to its large subunit at 17/19 kDa, and cleavage of Poly-ADP ribose polymerase (PARP) from 116 kDa to signature fragment of 89 kDa. Accumulation of cleaved PARP and the decrease of intact caspase-3 were observed in the PAA concentration-dependent manner, indicating that PAA-induced apoptosis was channeled through caspase-3 (Fig. 2C).

To explore the apoptosis mechanism upstream caspase-3, we examined the activation of different apoptotic markers. Mitochondria-mediated apoptosis pathway was characterized by up-regulated main pro-apoptotic protein Bax and down-regulated Bcl-2 expression [31]. Expression levels of Bax and anti-apoptotic regulator Bcl-2 were firstly assessed. Western blot analysis demonstrated that PAA administration induced the down-regulation of Bax and the Bcl-2 expression levels slightly increased (Fig. 2C), disproving the intrinsic mitochondria-mediated Bax/Bcl-2 apoptotic pathway. Our data suggested that PAA-induced apoptosis was initiated through other mechanism. This raised the question whether PAA triggered the extrinsic apoptotic pathway. Caspase-8 is the essential mediator of the extrinsic apoptotic pathway [32]. Cleaved caspase-8 (43 kDa) was accumulated as the increase of the PAA concentration, and accompanied with the decreased levels of the intact caspase-8 (Fig. 2C), indicating the activation of caspase-8 which led to the initiation of caspase-3. These results led us to hypothesize that PAA-induced apoptosis was channeled through caspase-8/caspase-3 pathway.

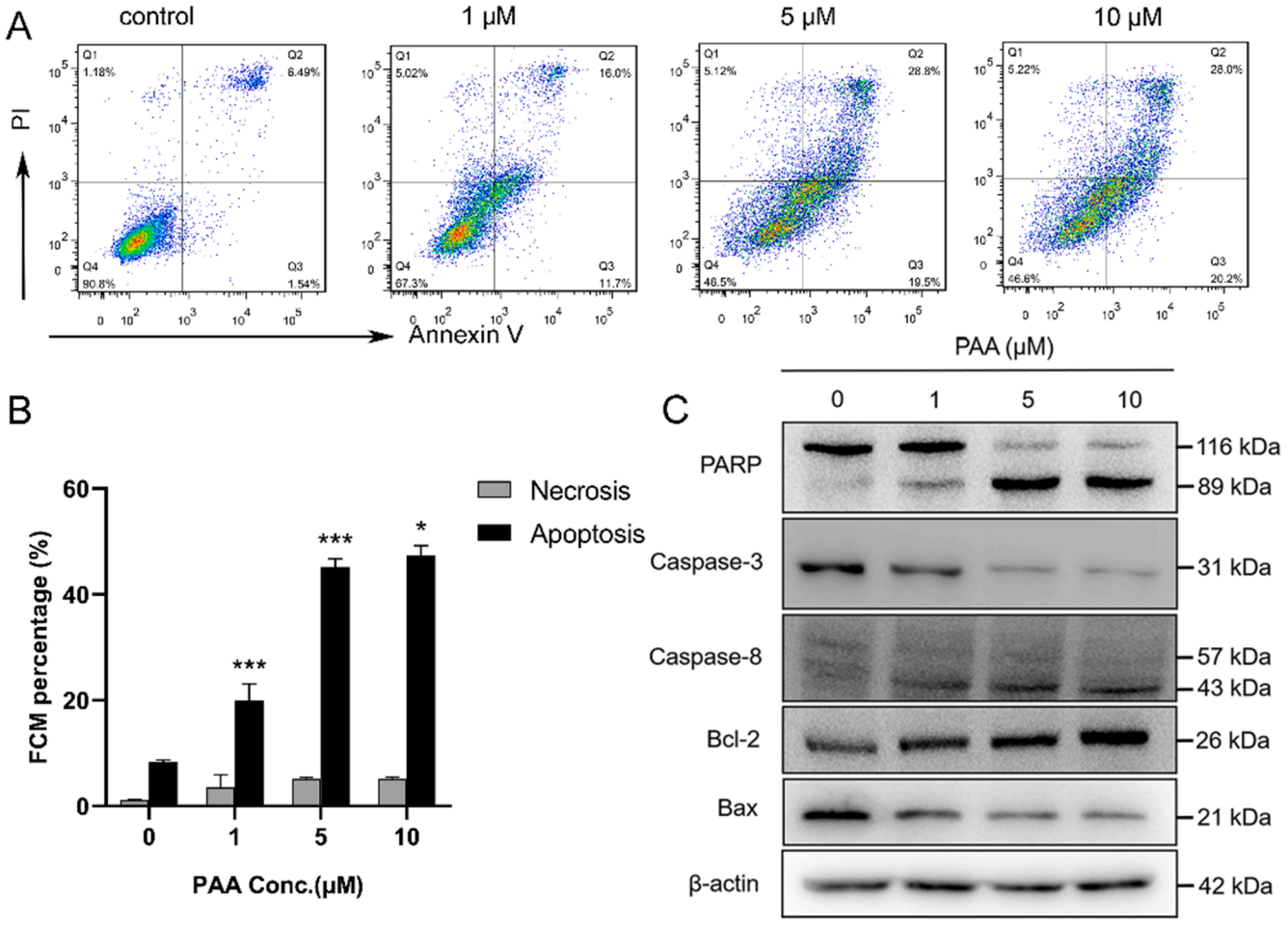

Fig. 2. PAA stimulates apoptosis mainly through caspase 8/caspase 3 pathway in HeLa cells. (A) PAA stimulates cell death. HeLa cells were treated with different concentrations of PAA and double stained with Annexin V-FITC and PI prior to flow cytometric analysis. Percentages of cells are denoted in each quadrant. The lower right and upper right quadrant represent early apoptotic and late apoptotic cells, respectively. The lower and upper left stands for the live and necrotic cells, respectively. (B) Bar graph representing the populations of HeLa cells in apoptosis and necrosis after treatment of PAA. Values of apoptotic cells are the sum of the lower and upper right quadrants and expressed from three independent experiments. (p value * < 0.05, ** < 0.01, *** < 0.001), vs previous data point. (C) Expression levels of apoptosis linked molecules in HeLa cells after PAA treatment.

2.3. Hypothesis and identification of PAA as a new Hsp90 inhibitor

During the mechanism study of anticancer activity, the expression profiles of a series of proteins involved with cell cycle distribution were investigated. Depletion of the Hsp90-dependent client proteins, including Akt kinase and CDK4, was also obvious (Fig. 3B). Interestingly, PAA also induced the increase of chaperon proteins levels, including Hsp27 and Hsp70 (Fig. 3B). Similar patterns of cellular response were observed in the liver hepatocellular (HepG2) cell after PAA treatment (Figure S2). Compensatory induction of the cytoprotective chaperons Hsp70 and Hsp27, and client protein depletion, comprise the most reliable biomarker signature event of Hsp90 inhibition and have been acknowledged in the clinical evaluation. In this regard, we speculated that PAA was possibly a new Hsp90 inhibitor.

Next, nuclear magnetic resonance (NMR) saturation transfer difference (STD) assay and surface plasmon resonance (SPR) were used to test the hypothesis. NMR STD assay generally investigates whether small molecules can interact with specific drug target and demonstrates the ligand binding epitope, providing information about the relative position of the compound with respect to the protein [33]. The collected NMR reference spectrum and STD difference spectrum (reflecting the STD effects) were overlapped and normalized with the signal H-1′, which exhibited the strongest STD enhancement. The zoomed in spectra focus on the methyl groups of PAA were shown in Fig. 3C. Protons closest to the protein surface showed the strongest STD effect. STD effect of H-1′, H-19 and H-17 (100%, 89% and 79%, respectively) suggest that these protons were in direct contact with Hsp90 surface. H−12 was possibly not in direct contact with Hsp90. Both NMR STD and SPR experiment confirmed the direct interaction between PAA and Hsp90 (Fig. 3D).

The initial finding inspired us to conduct Hsp90-dependent refolding and renaturation of luciferase assay to investigate the Hsp90 inhibitory activity of PAA. This assay detects whether compounds can inhibit the chaperon activity of Hsp90 by directing binding to its *N*-terminal or C-terminal domains [34]. PAA was shown to inhibit the renaturation of the luciferase and confirmed to be a Hsp90 inhibitor (Fig. 4A). Taken together, the aforementioned biochemical data confidently support that PAA directly interacts with Hsp90 and is a new Hsp90 inhibitor.

2.4. Synthesis and biological evaluation of photoaffinity-based chemical probe

To further investigate whether PAA binds to cellular Hsp90, we set ought to design chemical probe to pull down PAA binding proteins. NMR STD experiment suggested that H-1′ and H-19 exhibiting the strong STD enhancement interacts most with the protein surface, with C-18 carboxyl spatially far away from the interaction core (Fig. 3A). We speculated that modification of C-18 would not affect the Hsp90 inhibitory activity. To test our hypothesis, we designed, synthesized C-18 amide derivatives (**2**, **3**, **4**) (Scheme 1A and supplementary method), and assayed their Hsp90 inhibitory activity through Hsp90-dependent firefly luciferase refolding assay. As we expected, the derivatives **2**, **3** and **4** demonstrated similar Hsp90 inhibitory activity as that of PAA (Fig. 4), suggesting that C-18 amide derivatives retained the Hsp90 inhibitory activity. Consequently, we set out to design PAA-probe by introducing terminal alkyne and diazirine photoreactive moiety into the C-18 position of PAA. The PAA-probe was synthesized by following previously reported procedures with minor modification [35,36], with control-probe as a negative control (Scheme 1B). Cytotoxicity assay and Hsp90-dependent refolding of luciferase assay showed that PAA-probe exhibited similar anticancer and Hsp90 inhibitory activities (Table 1 and Fig. 4), strongly supporting that PAA-probe exhibited similar

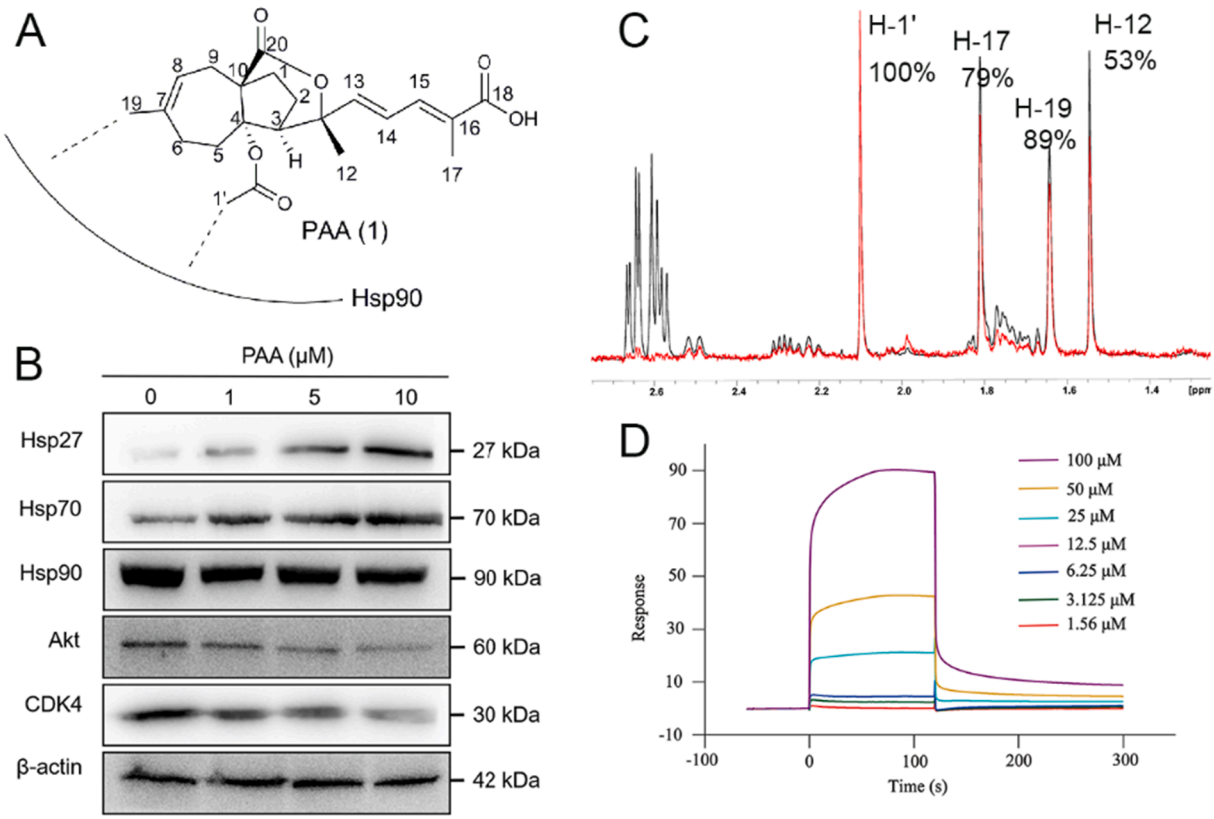

Fig. 3. PAA as a Hsp90 inhibitor and its binding to Hsp90. (A) Chemical structure of PAA and its relative orientation with Hsp90 revealed by NMR STD assay. (B) Cellular effect of PAA. Western blot analyses of the HeLa cell lysate after PAA treatment. (C) NMR STD assay. The overlaid ^{1}H spectra are reference spectrum (black) and STD difference spectrum (red), respectively, normalized with H-1′. (D) The SPR sensor gram (relative units (RU)) of PAA binding to Hsp90-immobilized chip. (For interpretation of the references to colour in this figure legend, the reader is referred to the web version of this article.)

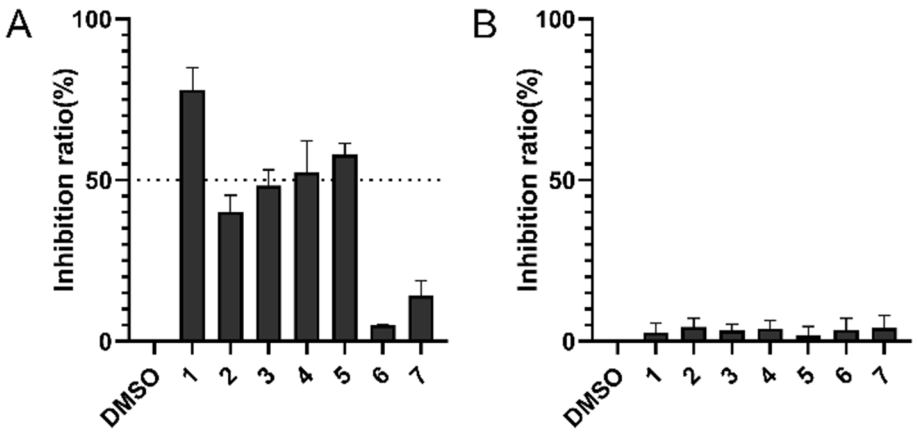

Fig. 4. (A) Hsp90 inhibitory activity of PAA and derivatives through Hsp90-dependent firefly luciferase renaturation assay. (B) All compounds did not inhibit native luciferase activity. The results are representative of three independent experiments.

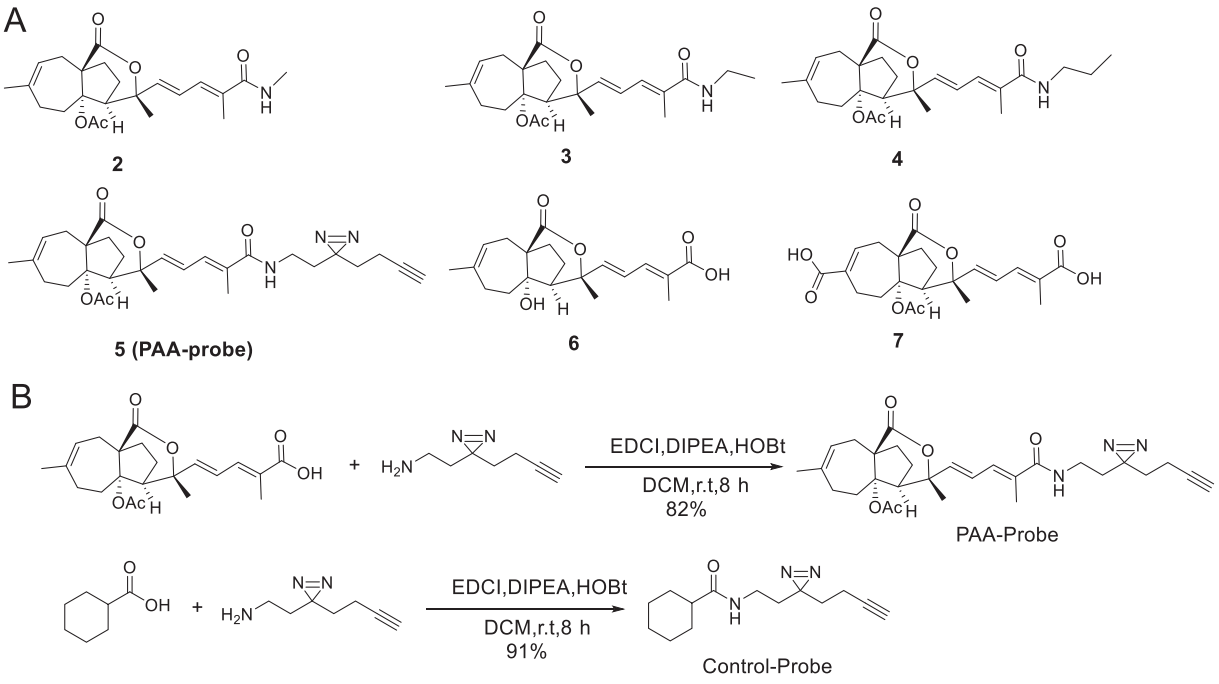

Scheme 1. (A) Chemical structures of PAA derivatives. (B) Synthetic scheme for PAA-probe and control-probe.

Table 1
IC_{50} values of PAA and its derivatives against five cancer cell lines.

IC_{50} (μM) [a]					
Compd.	HL-60	A549	SMMC-7721	HeLa	SW480
PAA	0.60 ± 0.01	2.72 ± 0.55	1.36 ± 0.05	2.92 ± 0.09	6.16 ± 0.59
2	1.35 ± 0.01	1.93 ± 0.31	1.27 ± 0.03	2.83 ± 0.12	10.43 ± 0.99
3	1.66 ± 0.07	4.05 ± 0.63	1.28 ± 0.05	4.06 ± 0.28	29.90 ± 1.76
4	1.69 ± 0.08	4.69 ± 0.11	1.40 ± 0.10	3.89 ± 0.25	33.25 ± 0.58
5	0.16 ± 0.01	4.62 ± 0.29	0.52 ± 0.01	3.25 ± 0.11	8.32 ± 0.20
6	> 40	> 40	> 40	> 40	>40
7	> 40	> 40	> 40	> 40	>40

[a] IC_{50} values are presented as mean ± SD of three independent experiments (SD is standard deviation).

function as PAA with regard to the activity and potency.

Next, we assessed the labeling effect of the PAA-probe with purified recombinant Hsp90 and conducted the competition assay. The PAA-probe could be further appended with the fluorescent dye (TAMRA) or a biotin moiety (TAMRA-Biotin-N_3) through click chemistry, which allowed the PAA interacting targets to be visualized on the gel or be enriched for pull down [37]. Results showed that fluorescence intensity increased as the concentration of probe increased (Fig. 5A). Maximum labeling was achieved at the PAA-probe concentration of 10 μM. Furthermore, competitive assay showed that the fluorescence intensity became weaker upon treatment with excess free PAA compound in the concentration dependent manner (Fig. 5B), indicating that the labeling of PAA-probe with Hsp90 was attributed by the PAA parental compound. Taken together, PAA-probe retained the Hsp90 binding activity.

2.5. PAA mainly binds to Hsp90 in HeLa cells using photoaffinity labeling approach

To investigate the *in vitro* interaction between PAA and Hsp90, the

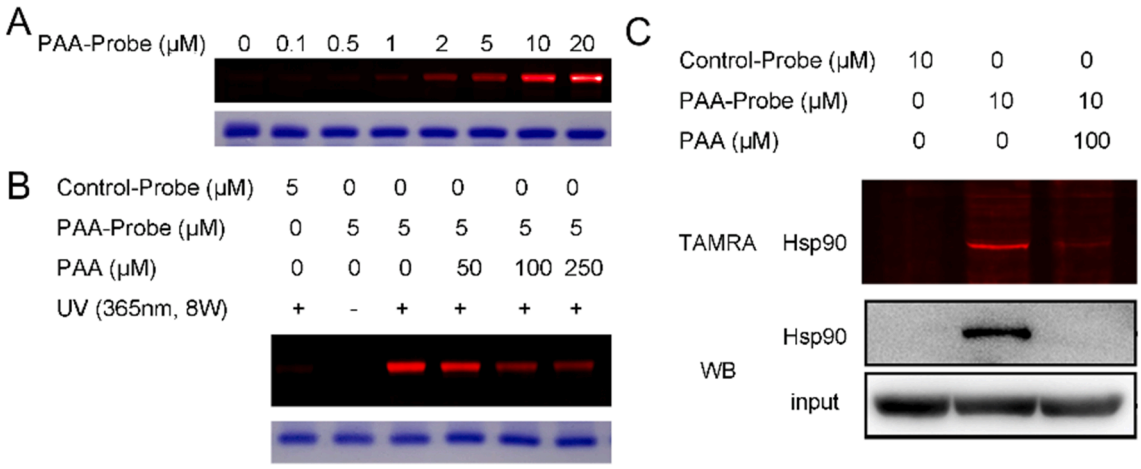

Fig. 5. PAA binds to Hsp90 in HeLa cells. (A) Labeling the purified recombinant Hsp90 by PAA-probe in the concentration-dependent manner. The coomassie brilliant blue (CBB) staining indicated that an equal amount of protein was loaded in each lane. (B) Competition assay. Purified Hsp90 was incubated with different concentrations of PAA and PAA-probe. The binding of Hsp90 with PAA-probe was competitively inhibited by the free compound PAA in the dose-dependent manner. (C) Validation of Hsp90 as the PAA cellular targets using pull down, in-gel fluorescence analysis (upper panel), and WB analysis (lower panel).

labeling of cell lysate, pull-down assay for enrichment of the cellular targets, and in-gel fluorescence assay were conducted using the PAA-probe and TAMRA-Biotin-N_3. The parallel experiment was performed with control-probe to indicate the cross-linker binders. In-gel based fluorescence indicated that the dominant band was about ~90 kDa, which was weakened by excess amount of compound PAA (Fig. 5C). The main fluorescently labeled band was further identified to be Hsp90 by western blotting (WB) experiments (Fig. 5C), confirming that PAA directly binds to cellular Hsp90.

2.6. PAA binds to the N-terminal domain of Hsp90

To identify the regions of Hsp90 involved in the interaction with PAA, a series of recombinant *N*-terminal domain (NTD) and C-terminal domain (CTD) of Hsp90 were constructed. NMR chemical shift perturbation assay, one of the most widely used NMR method to study protein-ligand interaction, was carried out to investigate the interaction with PAA [38]. A superimposition of the transverse relaxation optimized spectroscopy (TROSY) - heteronuclear single-quantum coherence (HSQC) spectra in the absence and presence of PAA was shown in Fig. 6 and Figure S3. Hsp90 CTD did not show detectable chemical shift perturbation upon titration of PAA (Figure S3), suggesting no interaction between CTD and PAA. Several peaks showed considerably chemical shift perturbations and intensity attenuation in the ^{1}H-^{15}N HSQC spectrum of NTD upon titration of PAA, indicating that these residues were involved in the direct interaction. Taken together, we concluded that PAA bind to the *N*-terminal domain of Hsp90, not the CTD.

Using previous assignment [39,40], Gly97 and Val148 were accurately assigned and identified among the residues with obvious chemical shift perturbations, suggesting their involvement in the interaction. Meanwhile, PAA-probe labeled Hsp90 sample was subjected to high resolution MS/MS analysis to reveal potential binding site. Results indicated that peptide TLTLVDTGIGMTK (residues 88–100) bind to PAA with highest possibility and confidence, further confirming that residue Gly97 and neighboring residues are responsible for PAA binding. Molecular docking analysis illustrated the NTD-PAA binding mode and showed that PAA inserted deeply into the cavity on the surface of Hsp90 NTD and directly interact with peptide TLTLVDTGIGMTK (Fig. 6B), which further supported the NMR titration and mass spectrometry results. Meanwhile, the model suggested that the C-19 terminal fragments buried inside the pocket and C-18 terminus pointed away from the pocket, consistent with the results of NMR STD assay. Taken these lines of data together, we concluded that Gly97, Val148, and residues

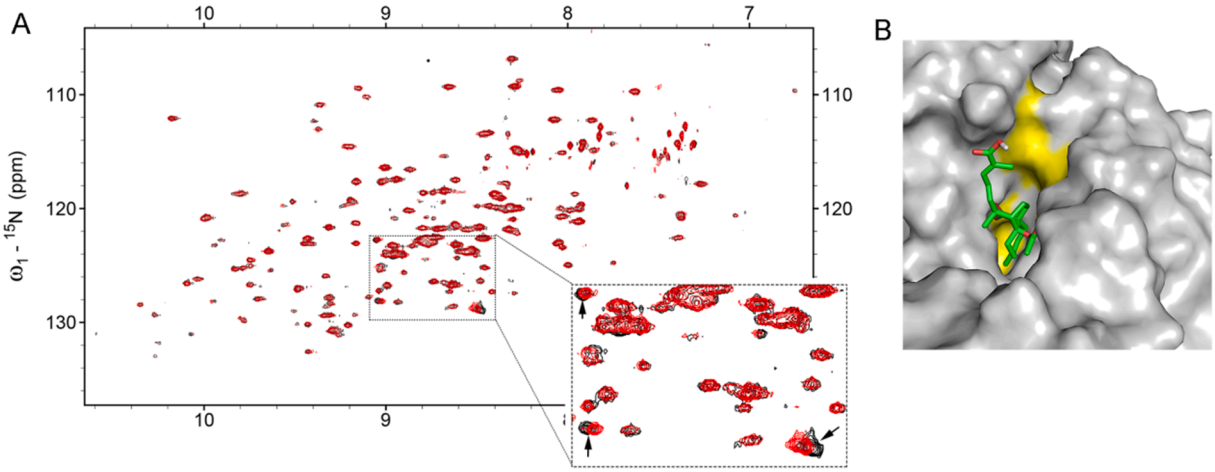

Fig. 6. *N*-terminal domain of Hsp90 is responsible for binding to PAA. A. Overlay of ^{15}N-^{1}H HSQC spectra of NTD in the apo form (black) and in the presence of compound PAA with the protein to peptide molar ratio of 1:2 (red). Black arrow in the zoom-in area indicates perturbations at selected residues. B. Molecular docking of PAA in complex with Hsp90 NTD. PAA is depicted in green. The peptide fragment identified by MS was colored in yellow.

spatially close to ATP binding pocket cavity of Hsp90 NTD were involved in the binding to PAA.

2.7. Correlation between Hsp90 inhibition and anticancer activity of PAA

Key challenge after target identification was to explore the connection between target engagement and anticancer activity of PAA. SAR study may shed some light. A series of C-4 and C-19 derivatives were synthesized and further assayed for the anticancer and Hsp90 inhibitory activities. C-4 deacetylated derivative **6** and C-19 carboxylic acid derivative **7** totally lost the Hsp90 inhibitory activity (Fig. 4). Consistently, they showed no anticancer activity ($IC_{50} > 40$ μM) (Table 1). C-18 amide derivatives (**2**, **3**, **4** and **5**) retained similar Hsp90 inhibitory activity, and concomitantly reserved similar anticancer activity (Table 1). These lines of data strongly support that the anticancer activity of PAA is correlated with the Hsp90 inhibitory activity.

A series of data including NMR STD, SAR and molecular docking analysis corroborate the notion that C-4 acetoxy group is essential for the activity and removal of the bulky group (**6**) abolishes Hsp90 binding activity and anticancer activity. C-19 allowed limited modifications. Derivative **8** with C-19 methylol group maintained the Hsp90 inhibitory activity (Figure S4). However, the bulky group such as carboxylic acid group (**7**) and methyl carboxylate group (PAB, **9**) is detrimental to the activity. Docking analysis showed that any C-19 group larger than methylol group would abolish other hydrogen bond and hydrophobic interactions with the residues of Hsp90 (Figure S4), resulting in the destabilization of small molecule in the pocket and loss of activity. Consistency of the Hsp90 inhibitory activity and cytotoxicity strengthens the notion that anticancer activity of PAA is correlated to its Hsp90 inhibitory activity.

PAA inhibits the function of Hsp90, leading to the degradation of CDK4 and Akt which are the client proteins of Hsp90 and highly involved in regulating the cell cycle. The PAA-induced depletion of CDK4 and Akt resulted in the activation of the checkpoints and the cell cycle blocking at G2/M phase, potentiating the cell proliferation suppression and cell death. These observations provided evidences to support the concept that the cellular consequence of Hsp90 inhibitory activity of PAA, including cell cycle arrest and apoptosis, is one of the possible mechanisms responsible for the anticancer activity of PAA.

PAA biochemically binds to the *N*-terminal domain of Hsp90. The *N*-terminal beta-strand and lid segments including residues 94–130 show high degree of mobility and large fluctuation [41,42], which is important for PAA binding and modulation of Hsp90 functions. In addition to Hsp90 *N*-terminal inhibitors, allosteric inhibitors targeting regions different from the active sites, such as the middle domain, C-terminal domain or the interface region of Hsp90, has emerged as a complementary strategy[29,43]. Selective inhibitors targeting specific Hsp90 PPIs without significant inhibition of all chaperon clients also provide new opportunities for drug development [44].

3. Conclusion

In summary, mechanistic studies showed that PAA displayed potent anticancer activity through inducing cell cycle arrest at G2/M phase and apoptosis. PAA directly binds to *N*-terminal domain of Hsp90 and is a new Hsp90 inhibitor. Through introducing the photoaffinity and terminal alkyne tag to parent PAA and generating the PAA-probe, which exhibits comparable efficacy as PAA, we confirmed the Hsp90-PAA interaction in HeLa cells and provided a photoactive probe for further exploring other potential targets. The anti-cancer activity of PAA is well correlated to its Hsp90 inhibitory activity and its cellular effect. Taking these lines of data together, we reveal one of the possible mechanisms by which the folk medicine achieves the anticancer activity through target identification strategy.

4. Materials and methods

4.1. Chemistry

Synthetic procedure and characterization of PAA derivatives including ^{1}H and ^{13}C NMR spectra were presented in Supporting information -Chemistry

4.2. Cell cycle analysis

Human cervical carcinoma HeLa cells (1×10^{6} cells/well in 6-well plates) were incubated with PAA (0, 0.1, 0.5, 1, 5 and 10 μM) for 16 h. The cells were washed, digested with EDTA-free trypsin. Harvested cells were resuspended in 75% ice-cold ethanol for 3 h at 4 °C. Fixed cells were resuspended in 500 μL PBS containing 10% RNase A and 11.6 μg/mL propidium iodide, and then incubated in the dark for 1 h. The cells were passed through a 70 μm griddle to exclude clustered cells. The percentage of cells at each phase of the cell cycle was analyzed by the FACS Calibur flow cytometer (BD Biosciences, Franklin Lakes, NJ). Data were processed using the software FlowJo 7.6.1.

4.3. Apoptosis analysis

HeLa cells were cultured as aforementioned. After incubated with the indicated compound (PAA (0, 1, 5, 10 μM)) for 16 h, the cells were harvested and stained with Annexin V-FITC/propidium iodide (PI). Annexin V shows a strong affinity in binding to phosphatidylserine in a Ca^{2+}-dependent manner and thus it is generally used as a probe to detect apoptosis. The apoptotic cells were counted after staining using an Annexin V-FITC/ PI apoptosis assay kit following the manufacturer's instructions. The collected cells were resuspended with 500 μL binding buffer. 5 μL Annexin V-FITC and 5 μL PI were added respectively, and then incubated in the dark for 15 min. The percentage of cells in different states was analyzed by the FACS Calibur flow cytometer (BD Biosciences, Franklin Lakes, NJ). Data were processed using the software FlowJo 7.6.1.

4.4. Western blotting analysis of whole-cell lysate

The HeLa cells were harvested in ice-cold lysis buffer (50 mM HEPES pH 8.0, 150 mM NaCl, 0.1 mM EDTA, 0.1% Triton X-100 and complete protease inhibitors) after incubation with different concentrations of PAA (0, 1, 5 and 10 μM) for 16 h. Protein concentrations of whole-cell lysate were measured using the BCA protein assay kit. Equal amounts of cell lysates were loaded to SDS-PAGE, transferred to PVDF membrane (Millipore) for 1 h. The membrane was blocked with buffer containing 5% non-fat milk, and incubated with the indicated primary antibodies at 4 °C overnight. Antibodies included HER2/ErbB2, p-Akt, Akt, CDK4, Hsp90, Hsp70, Hsp27, Beclin, β-actin, β- tubulin, PARP, Bcl-2, Bax, Caspase-3 and Caspase-8 (Cell Signaling Technologies, Boston, MA). The binding of antibody was visualized by peroxidase-conjugated secondary antibodies (anti-mouse or anti-rabbit) using the enhanced chemiluminescence, including Goat Anti-Mouse IgG (H + L)-HRP Conjugated and Goat Anti-Rabbit IgG (H + L)-HRP Conjugated (Coolaber Science and Technology Co., Ltd). β-actin was used as the loading control.

4.5. Protein expression and purification

Full length and different fragments (residues 17–223, 293–554 and 550–699, respectively) of Hsp90 were overexpressed in *E. coli* BL21 (DE3). Cell cultures were induced with 0.6 mM isopropyl β-D-thiogalactopyranoside (IPTG) at 37 °C for 4 h when the OD_{600} reached 0.6–0.8. The harvested cells were first passed through Ni-NTA affinity column and further purified by size-exclusion chromatography (Superdex 200, GE healthcare Life Sciences). The final protein sample was detected by SDS-PAGE and the purity is above 95%.

4.6. NMR STD assay and chemical shift titration assay

The NMR STD experiment was conducted on a Bruker Fourier spectrometer (800 MHz) at 298 K. The NMR sample contained 0.5 mM PAA in the absence or presence of the Hsp90 protein (10 μM). The NMR buffer is PBS buffer in 90% D_2O, pH7.4, with 1 mM DTT and 2.5% DMSO-d_6. The experiments were collected with a carrier set at −0.5 ppm for the on-resonance and −40 ppm for the off-resonance irradiation. The interaction between protein and the small molecule resulted in the saturation transfer and the signal intensity of the ^{1}H spectrum of the PAA decreased. The intensity difference was quantified using the equation $STD_{effect} = (I_o - I_{sat})/ I_o$, whereas I_o is the off-resonance signal intensity (reference spectrum), and I_{sat} is the intensity of the same signal in the on-resonance spectrum.

NMR chemical shift titration experiments were performed as described previously [45]. *N*-terminal domain (NTD) and C-terminal domain (CTD) of Hsp90 proteins were expressed in M9 minimal medium supplemented with $^{15}NH_4Cl$ (1 g/l) and ^{15}N-labeled proteins were obtained. 2D ^{15}N-^{1}H HSQC of NTD or CTD protein was recorded in the apo form. Increasing concentrations of compound PAA was added to the protein sample till the ratio of protein to compound reaches 1:10. A series of ^{15}N-^{1}H HSQC spectra were recorded at different molar ratios. The distinctive cross-peaks with chemical shift perturbations were assigned and verified according to BMRB database under the accession number 7003 [40].

4.7. Cytotoxicity assay

Five tumor cell lines, including HL-60, A549, SMMC-7721, HeLa, and SW480 were used to evaluate the cytotoxic activity of PAA and its analogs. The growth inhibitory effect was measured by MTT assay. Briefly, the cells in 96-well plates were treated in triplicate with grade concentrations (0.064, 0.32, 1.6, 8 and 40 μM) of the compound for 48 h. MTT solution (5 mg/ml) was added to each well with the final concentration of 20%. The culture was then incubated for 4 h and measured by the spectrophotometry at 492 nm. The results were expressed in IC_{50} and calculated by the GraphPad Prism software (GraphPad, Inc., San Diego, CA). The mean IC_{50} was determined from the results of three independent tests.

4.8. Surface plasmon resonance (SPR) experiment

Protein for SPR was dialyzed against Biacore buffer (50 mM HEPES; pH 7.4, 150 mM NaCl and 0.005% (w/v) polysorbate 20) and then immobilized on a CM5 chip. Binding analysis was performed at room temperature using a Biacore T200 instrument with a blank channel as a negative control. Compounds were prepared in running buffer and tested at different concentrations using a two-fold dilution series. In general, a series of different compound concentrations were injected on to the chip for a period of 10 min followed by a dissociation time of 15 min. The signal with response unit (RU), subtracting the reference response from the blank cell, was proportional to the amount of compound bound to the immobilized Hsp90 protein or fragment protein. A set of sensorgrams at different concentrations of compound were obtained. Equilibrium dissociation constant (K_d) was derived by Biacore T200 Evaluation Software using Steady State analysis (Biacore, Uppsala, Sweden).

4.9. Hsp90-dependent luciferase refolding assay

Hsp90-dependent refolding of firefly luciferase in rabbit reticulocyte lysate assay to identify the Hsp90 inhibitors was carried out as previously described with minor modification [34]. Briefly, firefly luciferase was denatured by heating at 41 °C for 10mins. Compounds with diluted concentrations, positive control (Novobiocin), and negative control (1% hemoglobin and 4% bovine serum albumin, TBS/HbBSA) were added to the 96-well plate. Refolding mixture including the denatured luciferase and reticulocyte lysate was injected to each well. The renaturation system was incubated at room temperature for 3 h. Equal volume of luciferin substrate solution was added to the system and the luciferase activity was measured using the Perkin-Elmer EnVision plate reader. The concentration-dependent inhibition of luciferase refolding was used to measure the IC_{50} of PAA and its analogs. The vehicle control (2.5% DMSO) and negative control (TBS/HbBSA) were used as the limits for 0% and 100% inhibition respectively. Control assay to exclude the direct inhibitory activity towards the native luciferase was also carried out. All reactions were tested in triplicate and the set of experiments were repeated three times.

4.10. Labeling profile of purified Hsp90 and gel-based fluorescence

Different concentrations of PAA-Probe were incubated with purified recombinant HSP90 protein (0.15 mg/ml in PBS buffer) at room temperature for 30mins. After irradiated with UV (365 nm, 8 Watt) on ice for 20 min, the sample is added with 1% SDS, 0.25 μL each of TAMRA-N_3 (125 μM final, Lumiprobe), CuSO4 (1.25 mM final, Sigma), THPTA (Tris (3-hydroxypropyltriazolylmethyl) amine, 125 μM final, Sigma) and sodium ascorbate (1.25 mM final). Each reagent was freshly prepared. The reaction system was incubated for 1 h at room temperature and subjected to SDS-PAGE. The readout is visualized by in-gel fluorescence scanning by Amersham Typhoon Biomolecular Imager at 533 nm. The gel was subsequently stained with coomassie brilliant blue to indicate that an equal amount of protein was loaded in each lane. The visualized bands were cut out and subjected to mass spectrometry to reveal the potential binding sites of Hsp90.

4.11. Pull down and western blotting analysis

HeLa cells were grown in DMEM (Dulbecco's modified eagle medium) supplemented with 10% FBS (Fetal Bovine Serum), 1% of penicillin and streptomycin. Cells were harvested by trypsinization and centrifugation. The lysis buffer contained 50 mM HEPES pH 8.0, 150 mM NaCl, 0.1 mM EDTA, 0.1% Triton X-100 and complete protease inhibitors, 1% NP-40 and 1 mM DTT. Protein concentration of the cell lysate was assessed using the BCA assay. The equivalent amount of protein extract was prepared for the following click chemistry reaction and microcentrifuge tube-based pull downs.

4.12. Competition assay

To further confirm endogenous Hsp90 was directly pulled down by PAA, we performed competition assay using the compound PAA. Briefly, excess amount of PAA (50 μM) was mixed with the HeLa cell lysate for 30 min, followed by incubation with the probe PAA-Probe (5 μM) and the aforementioned pull down and western blot analysis.

Declaration of Competing Interest

The authors declare that they have no known competing financial interests or personal relationships that could have appeared to influence the work reported in this paper.

Acknowledgements

This work was finally supported by National Natural Science Foundation of China (no. 21778059, no. 21837003) and the Ten thousand-talents program of Yunnan Province to Jiangxin Liu.

Appendix A. Supplementary material

Supplementary data to this article can be found online at https://doi.org/10.1016/j.bioorg.2021.104963.

References

[1] D.J. Newman, G.M. Cragg, Natural Products as Sources of New Drugs over the Nearly Four Decades from 01/1981 to 09/2019, J. Nat. Prod. 83 (3) (2020) 770–803.

[2] M. Schenone, V. Dancik, B.K. Wagner, P.A. Clemons, Target identification and mechanism of action in chemical biology and drug discovery, Nat. Chem. Biol. 9 (4) (2013) 232–240.

[3] R.L. Davis, Mechanism of Action and Target Identification: A Matter of Timing in Drug Discovery, Iscience 23 (9) (2020).

[4] J.L. Liu, J. Lee, M.A.S. Hernandez, R. Mazitschek, U. Ozcan, Treatment of obesity with celastrol, Cell 161 (5) (2015) 999–1011.

[5] J. Wang, C.J. Zhang, W.N. Chia, C.C.Y. Loh, Z.J. Li, Y.M. Lee, Y.K. He, L.X. Yuan, T. K. Lim, M. Liu, C.X. Liew, Y.Q. Lee, J.B. Zhang, N.C. Lu, C.T. Lim, Z.C. Hua, B. Liu, H.M. Shen, K.S.W. Tan, Q.S. Lin, Haem-activated promiscuous targeting of artemisinin in Plasmodium falciparum, Nat. Commun. 6 (2015).

[6] S. Zhuang, Q. Li, L. Cai, C. Wang, X. Lei, Chemoproteomic profiling of bile acid interacting proteins, ACS Cent Sci 3 (5) (2017) 501–509.

[7] E. Smith, I. Collins, Photoaffinity labeling in target- and binding-site identification, Future Med Chem 7 (2) (2015) 159–183.

[8] D. Korovesis, N. Rufo, R. Derua, P. Agostinis, S.H.L. Verhelst, Kinase Photoaffinity Labeling Reveals Low Selectivity Profile of the IRE1 Targeting Imidazopyrazine-Based KIRA6 Inhibitor, ACS Chem. Biol. 15 (12) (2020) 3106–3111.

[9] M. Hasegawa, T. Miura, K. Kuzuya, A. Inoue, S.W. Ki, S. Horinouchi, T. Yoshida, T. Kunoh, K. Koseki, K. Mino, R. Sasaki, M. Yoshida, T. Mizukami, Identification of SAP155 as the Target of GEX1A (Herboxidiene), an Antitumor Natural Product, ACS Chem. Biol. 6 (3) (2011) 229–233.

[10] K. Lee, H.S. Ban, R. Naik, Y.S. Hong, S. Son, B.K. Kim, Y. Xia, K.B. Song, H.S. Lee, M. Won, Identification of Malate Dehydrogenase 2 as a Target Protein of the HIF-1 Inhibitor LW6 using Chemical Probes, Angew. Chem.-Int. Ed. 52 (39) (2013) 10286–10289.

[11] J. Kreuzer, N.C. Bach, D. Forler, S.A. Sieber, Target discovery of acivicin in cancer cells elucidates its mechanism of growth inhibition, Chem. Sci. 6 (1) (2015) 237–245.

[12] A.E. Speers, G.C. Adam, B.F. Cravatt, Activity-based protein profiling in vivo using a copper(I)-catalyzed azide-alkyne [3+2] cycloaddition, J. Am. Chem. Soc. 125 (16) (2003) 4686–4687.

[13] A.L. Harvey, R. Edrada-Ebel, R.J. Quinn, The re-emergence of natural products for drug discovery in the genomics era, Nat. Rev. Drug Discov. 14 (2) (2015) 111–129.

[14] S.X. Wu, R.S. Hu, G.L. Yang, Experimental, clinical and pharmacological studies on antifungal effect of *Pseudolarix cortex*, Chin. J. Dermatol. 8 (1) (1960) 18–25.

[15] P. Chiu, L.T. Leung, B.C.B. Ko, Pseudolaric acids: isolation, bioactivity and synthetic studies, Nat. Prod. Rep. 27 (7) (2010) 1066–1083.

[16] D.J. Pan, Z.L. Li, C.Q. Hu, K. Chen, J.J. Chang, K.H. Lee, The cytotoxic principles of pseudolarix-kaempferi: Pseudolaric acid-A and acid-B and related derivatives, Planta Med. 56 (4) (1990) 383–385.

[17] S.P. Yang, Y.J. Cai, B.L. Zhang, L.J. Tong, H. Xie, Y. Wu, L.P. Lin, J. Ding, J.M. Yue, Structural modification of an angiogenesis inhibitor discovered from traditional Chinese medicine and a structure-activity relationship study, J. Med. Chem. 51 (1) (2008) 77–85.

[18] K.H. Yim, T.L. Prince, S.W. Qu, F. Bai, P.A. Jennings, J.N. Onuchic, E. A. Theodorakis, L. Neckers, Gambogic acid identifies an isoform-specific druggable pocket in the middle domain of Hsp90 beta, Proc. Natl. Acad. Sci. USA 113 (33) (2016) 4801–4809.

[19] J. Trepel, M. Mollapour, G. Giaccone, L. Neckers, Targeting the dynamic HSP90 complex in cancer, Nat. Rev. Cancer 10 (8) (2010) 537–549.

[20] D. Hanahan, R.A. Weinberg, Hallmarks of cancer: the next generation, Cell 144 (5) (2011) 646–674.

[21] W. Liu, G.A. Vielhauer, J.M. Holzbeierlein, H. Zhao, S. Ghosh, D. Brown, E. Lee, B. S. Blagg, KU675, a concomitant heat-shock protein inhibitor of Hsp90 and Hsc70 that manifests isoform selectivity for Hsp90alpha in prostate cancer cells, Mol. Pharmacol. 88 (1) (2015) 121–130.

[22] E. Hervouet, M. Cheray, F.M. Vallette, P.F. Cartron, DNA methylation and apoptosis resistance in cancer cells, Cells 2 (3) (2013) 545–573.

[23] L. Whitesell, S.L. Lindquist, HSP90 and the chaperoning of cancer, Nat. Rev. Cancer 5 (10) (2005) 761–772.

[24] D.B. Solit, F.F. Zheng, M. Drobnjak, P.N. Munster, B. Higgins, D. Verbel, G. Heller, W. Tong, C. Cordon-Cardo, D.B. Agus, H.I. Scher, N. Rosen, 17-Allylamino-17-demethoxygeldanamycin induces the degradation of androgen receptor and HER-2/neu and inhibits the growth of prostate cancer xenografts, Clin. Cancer Res. 8 (5) (2002) 986–993.

[25] S.M. Roe, C. Prodromou, R. O'Brien, J.E. Ladbury, P.W. Piper, L.H. Pearl, Structural basis for inhibition of the Hsp90 molecular chaperone by the antitumor antibiotics radicicol and geldanamycin, J. Med. Chem. 42 (2) (1999) 260–266.

[26] S. Mohamady, M.I. Ismail, S.M. Mogheith, Y.M. Attia, S.D. Taylor, Discovery of 5-aryl-3-thiophen-2-yl-1H-pyrazoles as a new class of Hsp90 inhibitors in hepatocellular carcinoma, Bioorg. Chem. 94 (2020), 103433.

[27] L.D. Shao, J. Su, B. Ye, J.X. Liu, Z.L. Zuo, Y. Li, Y.Y. Wang, C. Xia, Q.S. Zhao, Design, synthesis, and biological activities of vibsanin B derivatives: a new class of HSP90 C-terminal inhibitors, J. Med. Chem. 60 (21) (2017) 9053–9066.

[28] G. Morra, G. Verkhivker, G. Colombo, Modeling signal propagation mechanisms and ligand-based conformational dynamics of the Hsp90 molecular chaperone full-length dimer, PLoS Comput. Biol. 5 (3) (2009), e1000323.

[29] A. Paladino, M.R. Woodford, S.J. Backe, R.A. Sager, P. Kancherla, M.A. Daneshvar, V.Z. Chen, D. Bourboulia, E.F. Ahanin, C. Prodromou, G. Bergamaschi, A. Strada, M. Cretich, A. Gori, M. Veronesi, T. Bandiera, R. Vanna, G. Bratslavsky, S. A. Serapian, M. Mollapour, G. Colombo, Chemical Perturbation of Oncogenic Protein Folding: from the Prediction of Locally Unstable Structures to the Design of Disruptors of Hsp90-Client Interactions, Chemistry 26 (43) (2020) 9459–9465.

[30] L.C. Crowley, B.J. Marfell, A.P. Scott, N.J. Waterhouse, Quantitation of Apoptosis and Necrosis by Annexin V Binding, Propidium Iodide Uptake, and Flow Cytometry, *Cold Spring Harb. Protoc.* 2016 (11) (2016).

[31] X.F. Gong, M.W. Wang, Z. Wu, S. Tashiro, S. Onodera, T. Ikejima, Pseudolaric acid B induces apoptosis via activation of c-Jun N-terminal kinase and caspase-3 in HeLa cells, Exp. Mol. Med. 36 (6) (2004) 551–556.

[32] P.H. Krammer, R. Arnold, I.N. Lavrik, Life and death in peripheral T cells, Nat. Rev. Immunol. 7 (7) (2007) 532–542.

[33] M. Mayer, B. Meyer, Group epitope mapping by saturation transfer difference NMR to identify segments of a ligand in direct contact with a protein receptor, J. Am. Chem. Soc. 123 (25) (2001) 6108–6117.

[34] L. Galam, M.K. Hadden, Z.Q. Ma, Q.Z. Ye, B.G. Yun, B.S.J. Blagg, R.L. Matts, High-throughput assay for the identification of Hsp90 inhibitors based on Hsp90-dependent refolding of firefly luciferase, Bioorg. Med. Chem. 15 (5) (2007) 1939–1946.

[35] Z. Li, P. Hao, L. Li, C.Y. Tan, X. Cheng, G.Y. Chen, S.K. Sze, H.M. Shen, S.Q. Yao, Design and synthesis of minimalist terminal alkyne-containing diazirine photo-crosslinkers and their incorporation into kinase inhibitors for cell- and tissue-based proteome profiling, Angew. Chem. Int. Ed. Engl. 52 (33) (2013) 8551–8556.

[36] Y.Q. Zhou, Z.A. Di, X.M. Li, Y.H. Shan, W. Li, H.C. Zhang, Y.L. Xiao, Chemical proteomics reveal CD147 as a functional target of pseudolaric acid B in human cancer cells, Chem. Commun. (Camb.) 53 (62) (2017) 8671–8674.

[37] P. Ciepla, A.D. Konitsiotis, R.A. Serwa, N. Masumoto, W.P. Leong, M.J. Dallman, A. I. Magee, E.W. Tate, New chemical probes targeting cholesterylation of Sonic Hedgehog in human cells and zebrafish, Chem Sci 5 (11) (2014) 4249–4259.

[38] A. Marintchev, D. Frueh, G. Wagner, NMR methods for studying protein-protein interactions involved in translation initiation, Trans. Initiat.: Reconstituted Syst. Biophys. Methods 430 (2007) 283.

[39] S.J. Park, M. Kostic, H.J. Dyson, Dynamic Interaction of Hsp90 with Its Client Protein p53, J. Mol. Biol. 411 (1) (2011) 158–173.

[40] D.M. Jacobs, T. Langer, B. Elshorst, K. Saxena, K.M. Fiebig, M. Vogtherr, H. Schwalbe, NMR backbone assignment of the N-terminal domain of human HSP90. J. Biomol. NMR 2006, 36, 52.

[41] A. Schulze, G. Beliu, D.A. Helmerich, J. Schubert, L.H. Pearl, C. Prodromou, H. Neuweiler, Cooperation of local motions in the Hsp90 molecular chaperone ATPase mechanism, Nat. Chem. Biol. 12 (8) (2016) 628–635.

[42] I. D'Annessa, S. Raniolo, V. Limongelli, D. Di Marino, G. Colombo, Ligand Binding, Unbinding, and Allosteric Effects: Deciphering Small-Molecule Modulation of HSP90, J. Chem. Theory Comput. 15 (11) (2019) 6368–6381.

[43] C. Sanchez-Martin, E. Moroni, M. Ferraro, C. Laquatra, G. Cannino, I. Masgras, A. Negro, P. Quadrelli, A. Rasola, G. Colombo, Rational Design of Allosteric and Selective Inhibitors of the Molecular Chaperone TRAP1, Cell Rep 31 (3) (2020), 107531.

[44] S.A. Serapian, G. Colombo, Designing Molecular Spanners to Throw in the Protein Networks, Chemistry 26 (21) (2020) 4656–4670.

[45] J.X. Liu, J.H. Zhang, Y.S. Yang, H.D. Huang, W.Q. Shen, Q. Hu, X.S. Wang, J.H. Wu, Y.Y. Shi, Conformational change upon ligand binding and dynamics of the PDZ domain from leukemia-associated Rho guanine nucleotide exchange factor, Protein Sci. 17 (6) (2008) 1003–1014.